In this issue

European Centre for Medium-Range Weather Forecasts

Shinfield Park, Reading, Berkshire RG2 9AX, UK

Fax: . . . . . +44 118 986 9450

Telephone: National 0118 949 9000

International . . . . . +44 118 949 9000

Public Web site . . . . . http://www.ecmwf.int

Member States' Web site . . . . . http://wms.ecmwf.int

Front Cover

ECMWF's wave-model products are outlined on page 9 of this issue.

Editorial

The new radiation-transfer scheme RRTM is described in the article on page 2. The new scheme includes the representation of sixteen spectral bands, compared with six bands in the previous operational scheme. This allows improvements in the spectral description of the radiative properties of both the earth's surface and the clouds. Tests of the impact of the scheme indicate improved anomaly correlations, particularly in the Southern Hemisphere.

On page 9 Jean Bidlot outlines the products that are now available from the ECMWF wave-model forecasts. A variety of parameters are output, both from a global version of the model having a grid length of 55km and from a limited area wave model covering the North Atlantic and the seas around Europe, which has a 28km grid.

Articles from recent issues of the Newsletter are now available from the ECMWF Web Site as pdf files (http://www.ecmwf.int/pressroom/newsletter/index.html). The index of past Newsletter articles printed at the end of each issue has now been reorganised to be consistent with the index on the Web Site. Articles that are available on the Web are indicated by asterisks.

Peter White

Changes to the Operational Forecasting System

Cycle 23r4 was implemented on 12 June 2001. This version includes several changes in the use of satellite data over land and sea ice (more AMSU data and the use of skin temperature rather than upper-layer soil temperature in processing radiances). In addition, the radiation parametrization routines are called on an hourly (instead of three-hourly) basis during the data assimilation. The time integration of the surface skin temperature over land has been improved. The horizontal diffusion of vorticity has been increased to bring it into line with that applied to the divergence and temperature, but without any noticeable impact on the forecast fields. Finally, an improved ozone model developed by Météo-France has been introduced with a new parametrization of the destruction of ozone by heterogeneous chemical processes. No meteorological impact (other than on the ozone fields themselves) is expected from this change.

Verification has shown a noticeable reduction in cold biases of the 2m temperature around sunset; this is linked to the improved time integration of land-surface temperature. The scores for the free atmosphere show a very minor, and overall neutral, impact of the changes on the performance during the three months of testing currently available.

Future Changes

Pre-operational testing will start over the summer for an important set of changes both to the data assimilation (T255 inner loops, new J_b statistics, new humidity structure functions, the use of water-vapour radiances from Meteosat and of sea winds from QuikSCAT, an upgrade of the radiative-transfer code, upgraded quality control for mobile platforms,

the use of extra channels from AMSU-A for an extended application of the data over land), and to the forecast model (finite elements in the vertical, a revised precipitation scheme, improvements in the oceanic wave model). □

François Lalaurette

Impact of the radiation-transfer scheme RRTM in the ECMWF forecasting system

From May 1989 to June 2000, the long-wave (LW) radiation scheme operational at the European Centre for Medium-Range Weather Forecasts (ECMWF) was a band-emissivity type scheme (*Morcrette*, 1991; *Gregory et al*, 1998; hereafter referred to as M91/G98). This LW scheme handles cloudiness using the effective-cloudiness approach. The availability of schemes based on more efficient solutions of the radiative-transfer equation (RTE), and of schemes validated, not only on line-by-line model results but also on actual spectrally detailed measurements available as part of the Atmospheric Radiation Measurements (ARM) program, made it timely to reconsider the way the LW radiation transfer was handled. Recently such a scheme, the Rapid Radiative Transfer Model (RRTM), developed at the Atmospheric and Environmental Research, Inc. USA (AER), was made available to ECMWF and was thoroughly tested in seasonal integrations with the ECMWF model (*Morcrette et al.*, 1998).

In contrast to the M91/G98 LW scheme, the RRTM allows the representation of both the true cloud fraction and the spectrally defined emissivities and transmissivities in each of the 16 different spectral bands. As the M91/G98 LW scheme considers only six bands, it is thus possible to improve on the spectral description of both the surface and the cloud radiative properties.

Various changes were made, both at AER and within ECMWF, to adapt the RRTM to the ECMWF computer environment. In the following, this version of the RRTM is referred to as RRTM_EC. It includes a change of the cloud overlap assumption, and the inclusion of the effects of aerosols and different sets of cloud optical properties. More than 150 T_L319 L60 forecasts have been run with RRTM_EC, either alone or as part of a package of modifications of the forecast system developed for the ECMWF 40-year reanalysis (ERA-40). This report presents an account of the impact of RRTM_EC on the analyses and ten-day forecasts with the ECMWF system. Analyses and ten-day forecasts are considered over the period 1 April to 15 May 1999, for which the impact of the improved representation of the LW radiation can be obtained in isolation from other modifications to the system.

In this article both LW radiation schemes are briefly described together with stand-alone one-dimensional comparisons of heating-rate profiles. Using the results of a six-week pre-operational testing programme of RRTM_EC within the full ECMWF forecast system, the impacts on the analyses and ten-day forecasts are discussed. The RRTM has been the operational LW radiation scheme since 27 June 2000.

The long-wave radiation-transfer schemes

Table 1 presents a summary of the characteristics of the two LW schemes discussed in the following sections.

Table 1 Characteristics of the long-wave radiation schemes

		RRTM	**M91/G98**
Solution of radiative-transfer equation		Two-stream method	Spectral emissivity method
Number of spectral intervals		16	6
Absorbers		H_2O, CO_2, O_3, CH_4, N_2O, CFC11, CFC12, aerosols	H_2O, CO_2, O_3, CH_4, N_2O, CFC11, CFC12, aerosols
Spectroscopic database		HITRAN 1996	HITRAN 1992
Absorption coefficients		From LBLRTM line-by-line model	Fits on statistical models of transmission
Cloud handling		True cloud fraction	Effective cloud fraction CF × ε
Cloud optical properties: method		16-band spectral emissivity	Whole spectrum emissivity
Data	Ice Clouds	*Ebert and Curry* (1992); *Fu et al.* (1998);	*Ebert and Curry* (1992)
	Water Clouds	*Smith and Shi* (1992) *Savijarvi and Raisanen* (1997)	*Smith and Shi* (1992);
Cloud overlap assumption		Maximum random	Maximum random (maximum and random also possible)
Reference		*Mlawer et al.* (1997)	*Morcrette et al.* (1986) *Morcrette* (1991) *Gregory et al.* (1998)

The M91/G98 code

The LW radiation scheme, operational at ECMWF from May 1989 to June 2000 (*Morcrette*, 1991) accounts for absorption by water vapour, carbon dioxide, ozone, methane, nitrous oxide, CFC-11, and CFC-12. It is based on an emissivity method in which the transmission functions for water vapour and carbon dioxide over the six spectral intervals of the scheme have been fitted using Pade approximants on narrow-band transmissions obtained with statistical band models. At the time of its development, it was validated against the Laboratoire de Météorologie Dynamique 4A line-by-line model. However, despite some updates to the absorption coefficients following the availability of newer versions of the database of spectroscopic parameters (from HITRAN'82 to HITRAN'86 to HITRAN'92), some of its features made it somewhat outdated, particularly its parametrization of the water-vapour continuum absorption based on *Roberts et al.* (1976). In consequence, a revision of the water-vapour continuum based on continuum measurements (CKD1) by *Clough et al.* (1992) was introduced as part of the December 1997 revision (cycle 18r3) of the physics package (*Gregory et al.*, 1998; hereafter G98). For the relevant spectral intervals of both schemes, ice-cloud optical properties are derived from the paper by *Ebert and Curry* (1992) and water-cloud optical properties from the paper by *Smith and Shi* (1992). In this scheme, semi-transparent clouds are treated using an effective cloud cover, the product of the actual cloud cover by the cloud emissivity computed for the whole LW spectrum.

The RRTM_EC

As stated by *Mlawer et al.* (1997), the objective in the development of the Rapid Radiation Transfer Model has been to obtain accuracy in the calculation of fluxes and cooling rates consistent with the best line-by-line models. It utilises the correlated-k method and shows its affiliation to the AER line-by-line model (*LBLRTM*, *Clough et al.*, 1989, 1992; *Clough and Iacono*, 1995) through its use of absorption coefficients for the relevant k-distributions derived from LBLRTM. Therefore, the k-coefficients in RRTM include the effect of the CKD2.3 water-vapour continuum (*Clough et al.*, 1989). The main point in the correlated-k method is the mapping of the absorption coefficient k(n) from the spectral space (where it varies irregularly with wave number n) to the g-space (where g(k) is the probability distribution function, i.e. the fraction of the absorption coefficients in the set smaller than k). The effect of this reordering is a rearrangement of the sequence of terms in the integral over wave number in the RTE, which makes it equivalent to what would be done for monochromatic radiation.

The accuracy of these absorption coefficients has been established by numerous and continuing high-resolution validations of LBLRTM with spectroscopic measurements, in particular those from the ARM. Compared with the original RRTM (*Mlawer et al.*, 1997), RRTM_EC was modified to account for cloud optical properties and surface emissivity defined for each of the 16 bands over which spectral fluxes are computed. For efficiency reason, the original number of g-points (256 = 16 × 16) has been reduced to 140. Other changes are the use of the CKD2.3 water-vapour continuum (instead of the CKD2.2 version of the original RRTM) and a diffusivity approximation (instead of the three-angle integration over the zenith angle used in the original scheme) to derive upward and downward fluxes from the radiances, and the modification of the original cloud random-overlapping assumption to include (to the same degree of approximation as used in the operational ECMWF SW scheme) a maximum random overlapping of cloud layers. Optical properties of clouds have been defined for both water and ice clouds in each of the 16 spectral intervals. Various sets of cloud optical properties are available for the RRTM and, while the better spectral definition of these coefficients will make them preferable in the future, the impact on the LW cloud optical thickness is relatively small. Results in the following are for optical properties from *Ebert and Curry* (1992) for ice clouds and from *Smith and Shi* (1992) for liquid-water clouds.

Given the monochromatic form of the RTE, the vertical integration is simply carried out one layer at a time from the top of the atmosphere (ToA) to the surface to get the downward fluxes. The downward fluxes at the surface are used with the spectral surface emissivities and the surface temperature to get the upward long-wave fluxes in each of the 140 subintervals. Then the upward fluxes are obtained in a similar fashion from the surface to ToA.

One-dimensional comparisons on standard atmospheres

Fluxes and cooling rates computed by the RRTM and LBLRTM have been compared by *Mlawer et al.* (1997), and show an agreement better than 0.5 Wm^{-2} on the fluxes at the surface and ToA, and better than 0.05 K day^{-1} in any layer over the vertical depth of the atmosphere. Here we compare fluxes and cooling rates from RRTM_EC to those from M91/G98.

Table 2 presents for the standard atmospheres of *McClatchey et al.* (1971) (tropical (TRO), mid-latitude summer (MLS) and winter (MLW), sub-arctic summer (SAS) and winter (SAW)) a comparison of the two LW schemes in stand-alone computations, for the clear-sky outgoing LW radiation (OLR) at the ToA and the downward long-wave radiation at the surface (SDLR). Figure 1 compares the LW heating

		TRO	MLS	MLW	SAS	SAW
OLR	RRTM_EC	286.2	276.2	226.6	257.7	196.1
	M91/G98	291.0	281.8	230.0	264.3	198.5
SDLR	RRTM_EC	399.3	350.5	224.3	301.1	173.9
	M91/G98	390.9	344.4	220.4	296.1	170.9

TRO – tropical;
MLS – mid-latitude summer;
MLW – mid-latitude winter;
SAS – sub-arctic summer;
SAW – sub-arctic winter.
All fluxes are in Wm^{-2} and the surface emissivity is 0.99.

Table 2 Boundary fluxes in clear-sky atmospheres

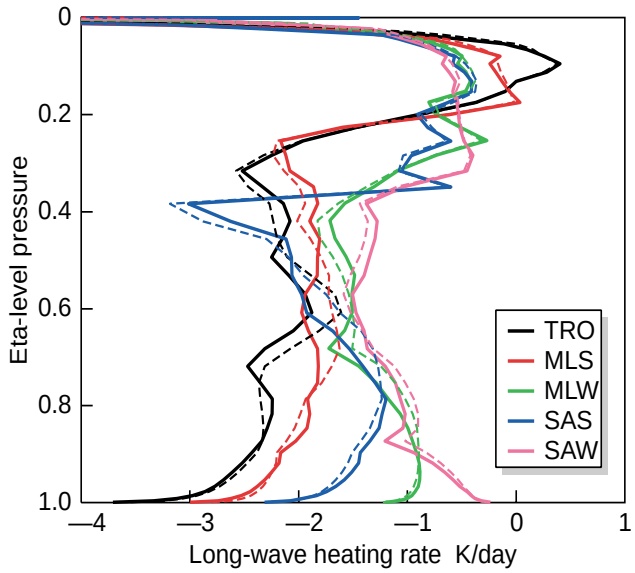

Figure 1 The clear-sky heating rate computed for the standard atmospheres by RRTM_EC (full lines) and M91/G98 (dashed lines).

rates for the standard atmospheres. The main difference between the two schemes is a decrease in the intensity of the maximum cooling that RRTM_EC brings to the clear-sky cooling rate for pressures between 200 and 500 hPa, an increase of the clear-sky cooling rate for pressures larger than 600 hPa down to about 900 hPa. This can be linked to the overall increase of the greenhouse effect of the long-wave absorption, related to the improvement and strengthening of the water-vapour p-type absorption, particularly important in the pure rotation part of the water-vapour spectrum around 30 μm. For the fluxes at the boundaries of the atmosphere, the increased opacity of the atmosphere due a better and more intense continuum absorption appears as a decrease in OLR and an increase in SDLR for all atmospheres. In terms of total clear-sky long-wave divergence, RRTM_EC increases it in TRO by 5.2 Wm^{-2} (from 223.8 with M91/G98 to 229.0 with RRTM_EC), down to 1.7 Wm^{-2} for SAW.

Table 3 presents similar diagnostics on fluxes at the boundaries when a low-level cloud (with 90% cover) is present between $\sigma = 0.78$ and 0.87 in the atmospheres, assuming a proportionality factor of 2% between the liquid-water mixing ratio and the saturation water-vapour mixing ratio. Results for such a cloud, with an emissivity at, or very close to, unity are similar to those for clear skies, so the impact of the increased continuum absorption is roughly similar to what is presented in Table 2. For that particular case, whether the optical properties are averaged (as in M91/G98) or spectrally defined (as in RRTM_EC) has very little impact. Results for sets of ice clouds embedded in the standard atmospheres are also presented in Table 3. For these comparisons, the high-level cloud is always located in the three layers just below the tropopause and is given a ice-water mixing ratio corresponding to 5% of the saturation mixing ratio of the layers in which it is embedded. The differences in fluxes at the

		TRO	MLS	MLW	SAS	SAW
90% low cloud						
OLR	RRTM_EC	275.0	267.8	220.5	249.7	197.7
	M91/G98	277.1	269.2	221.5	250.6	197.9
SDLR	RRTM_EC	440.2	406.3	293.5	363.4	240.4
	M91/G98	438.6	405.4	290.0	362.9	223.6
90% high cloud						
OLR	RRTM_EC	279.8	265.9	218.4	240.4	190.7
	M91/98	286.3	277.2	226.5	256.6	196.1
SDLR	RRTM_EC	399.6	351.2	226.3	304.1	176.2
	M91/G98	391.2	344.8	221.2	297.4	171.9

TRO - tropical;
MLS - mid-latitude summer;
MLW - mid-latitude winter;
SAS - sub-arctic summer;
SAW - sub-arctic winter.

All fluxes are in W m^{-2}. The low-level cloud is made of liquid water only with $q_{cloud} = 0.02\ q_{sat}$ and the water-cloud optical properties are from *Smith and Shi* (1992). The high-level cloud is made of ice water only with $q_{cloud} = 0.05\ q_{sat}$ and the ice-cloud optical properties are from *Ebert and Curry* (1992).

Table 3 Boundary fluxes for standard atmospheres with a low-level cloud or a high-level cloud below the tropopause

boundaries and heating-rate profiles (not shown) between the various sets of optical properties used with RRTM_EC are very similar. The difference from M91/G98 is usually larger, a result firstly of the separate treatment of the cloud fraction and the cloud-layer emissivity in RRTM_EC, and secondly of the cloud LW emissivity being spectrally averaged in M91/G98 and spectrally dependent in RRTM_EC.

Impact on analyses and first-guess forecasts

Analyses

Impact of RRTM_EC on analyses is mainly felt in the stratosphere for temperature (Figure 2), and right below the tropopause for temperature and humidity (Figure 3). The effect in the stratosphere is a "pure" radiative effect, with temperature adjusting to slightly different LW radiative heating, because RRTM_EC includes the full treatment of the Voigt line broadening present in the line-by-line model, whereas the M91/G98 scheme only has a more approximate treatment of the Voigt line profile (*Giorgetta and Morcrette*, 1995). In the tropics, the increased destabilisation provided by RRTM_EC in clear sky slightly enhances the convection, with the uppermost clouds moving up, thus creating the temperature dipole around 100 hPa, the increase in specific humidity close to the level of detrainment, and the change in cloud cover (Figure 4). The increased convection gives a slight increase in high cloudiness over the ITCZ and a slight decrease away from it. However, the impact on the wind remains small (not shown).

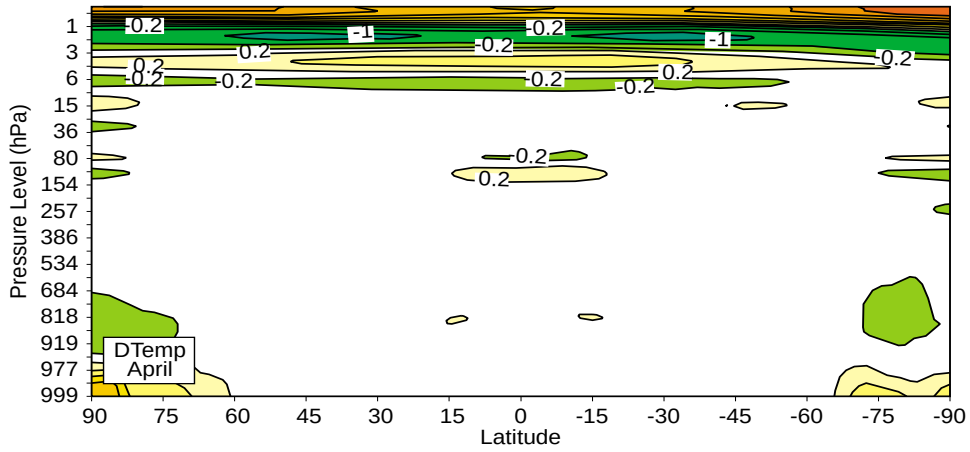

Figure 2 The difference in zonal mean temperature, for the month of April 1999, between the analyses including RRTM_EC and the one with M91/G98. Step is 0.4K starting from ±0.2 K.

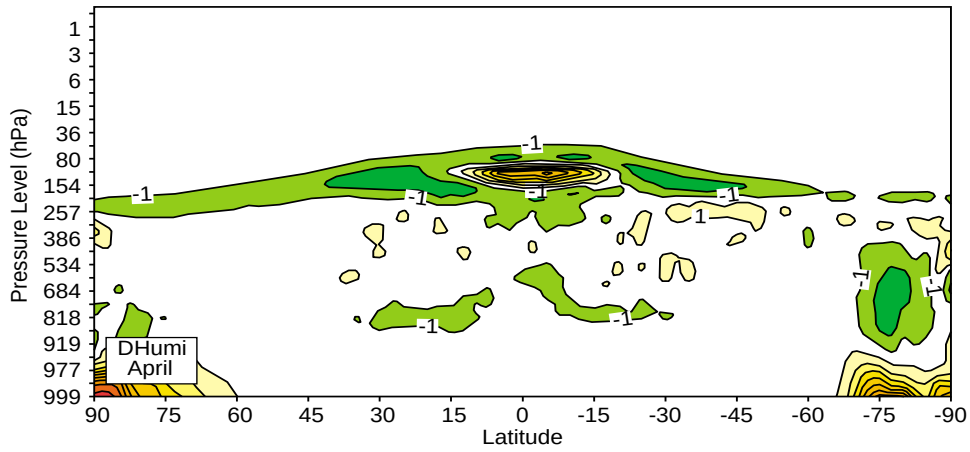

Figure 3 The relative difference in zonal mean specific humidity, for the month of April 1999, between the analyses including RRTM_EC and the one with M91/G98. In percent with a step of 2% starting from ±1%.

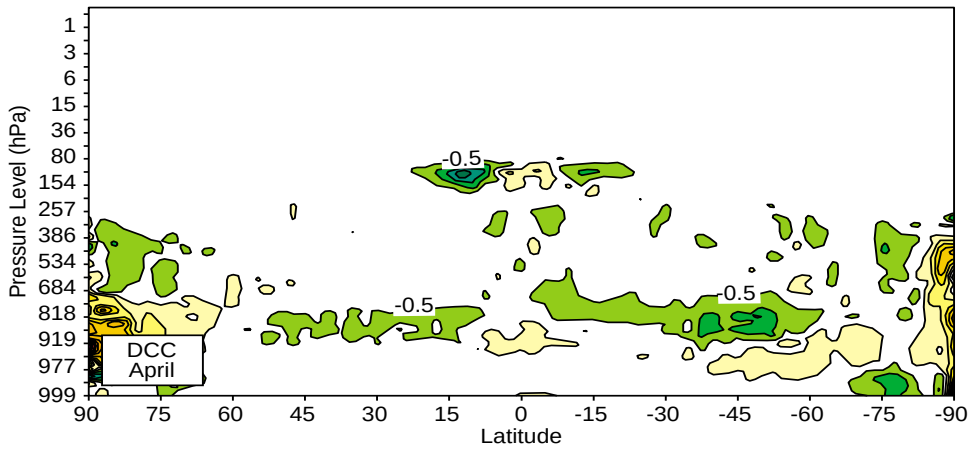

Figure 4 The difference in cloudiness, for the month of April 1999, between the 6-hour first-guess forecasts including RRTM_EC and those with M91/G98. Step is 1 percent starting from ±0.5%.

Comparison of first-guess downward LW radiation with surface observations.

The LW radiative fluxes, obtained during the six-hour first-guess forecasts by the ECMWF operational system, have been compared with a number of well-calibrated surface radiation measurements made as part of the Baseline Surface Radiation Network (*Ohmura et al*, 1998) over stations encompassing various climatic regimes from polar to tropical latitudes. Working with six-hour first-guess forecasts, when the model is still close to the analysed initial conditions, should help pinpoint the reasons for discrepancies between model and observations. Observational data are available for April and May 1999. All measuring stations have adopted the 5 Wm^{-2} standards for thermal infrared measurement set by BSRN. Although observations are available with a frequency of at least 3 min, all parameters have been averaged over three-hour periods within the six hours of the first-guess forecasts starting at 00, 06, 12 and 18 UTC. Over all stations, RRTM_EC generally increases the downward LW radiation, with maximum impact in either cold (Ny Alesund 79°N, 12°E, South Pole; Figure 5) or dry atmospheres. In moister atmospheres, the impact is still positive but appears smaller. This signal is seen in clear and cloudy atmospheres. In these comparisons, most of the discrepancies are related to problems in the cloudiness being not extensive enough, too high or too transparent.

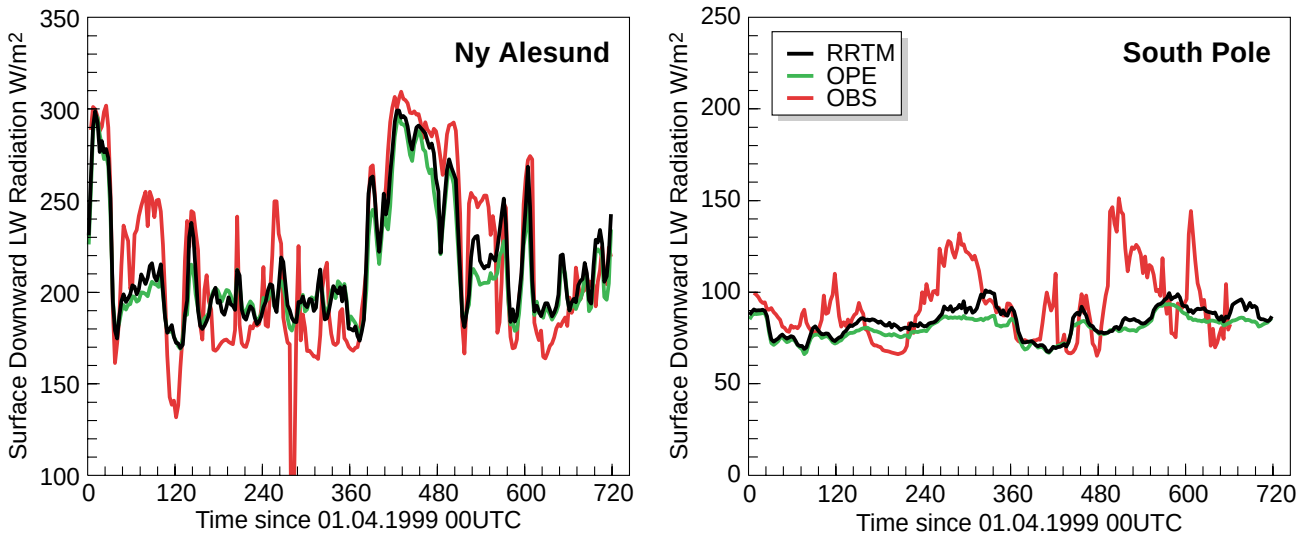

Figure 5 The downward long-wave radiation at the surface for the two high-latitude stations (left: Ny Alesund; right: South Pole) for April 1999. Model is derived from 3 and 6-hour first guess forecasts. EC-OPE includes M91/G98.

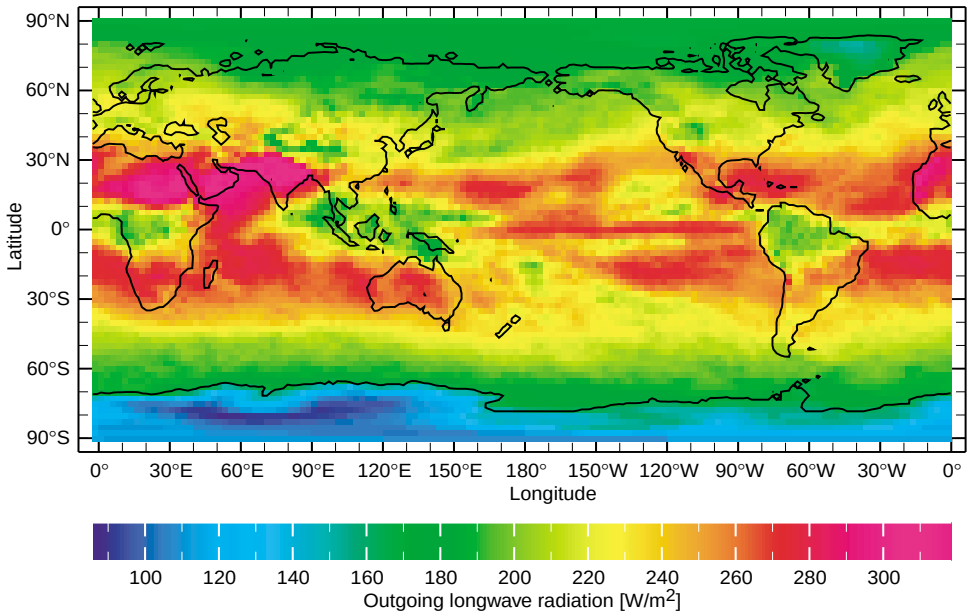

Figure 6 The outgoing LW radiation at the top of the atmosphere (in Wm^{-2}) observed during April 1999 (NCEP-CDC).

Impact on ten-day forecasts

LW radiation fields

Here we concentrate on the series of 45 T_L319 L60 ten-day forecasts run either with M91/G98 or RRTM_EC over the period 1 April to 15 May 1999. Figure 6 presents the OLR derived by the National Centers for Environmental Prediction Climate Data Center using a regression analysis on HIRS/2 radiances for April 1999. Figure 7 compares the OLR from the ensemble of the first 24-hour forecasts with either RRTM_EC or the M91/G98 LW radiation scheme. Part of the signal corresponds to the effect of the continuum absorption already seen for the initial clear-sky fields, this time modulated by the clouds. The main differences are in the distribution of the minimum OLR corresponding to cloudy areas that appear somewhat mislocated in both model simulations over the west Pacific, to the north of South America, the equatorial Atlantic and Africa. The overall agreement in mainly clear-sky areas is better, but the OLR over Antarctica appears too high and the OLR over western Sahara appears too low in the model compared with the HIRS/2-derived OLR. In the tropics, the net LW radiation at the surface (not shown) decreases (in absolute values) indicating an increase in the downward LW radiation. A similar increase in downward LW radiation is also seen at higher latitudes, coming from both clear-sky and cloudy situations.

Objective scores

Figure 8 compares the anomaly correlation for the geopotential at 500 hPa (Z500) for the northern and southern hemispheres and the European area for the set of 45 forecasts of the April to May 1999 experimentation period. Over the three areas, and over most of the forecast length,

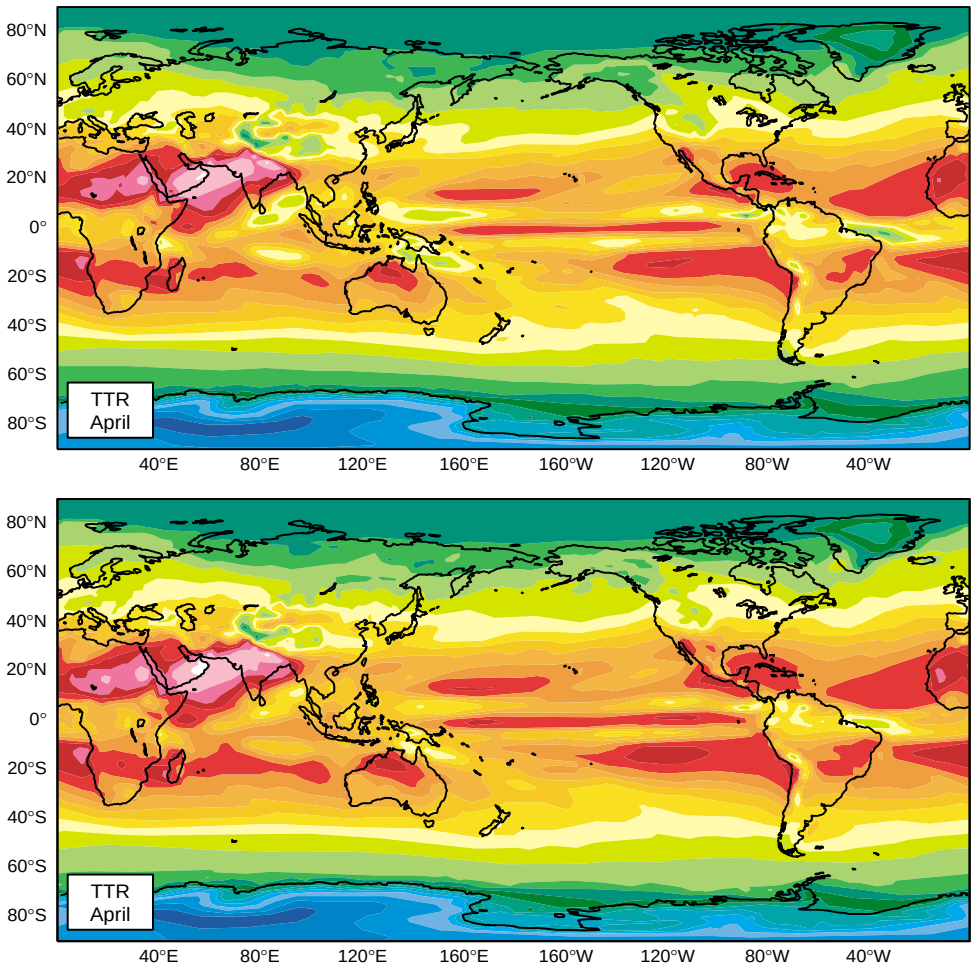

Figure 7 The outgoing long-wave radiation at the top of the atmosphere computed with the experimental suite model including RRTM_EC (top panel) and the operational model including M91/G98 (bottom panel). Colour scale is as in Fig. 6.

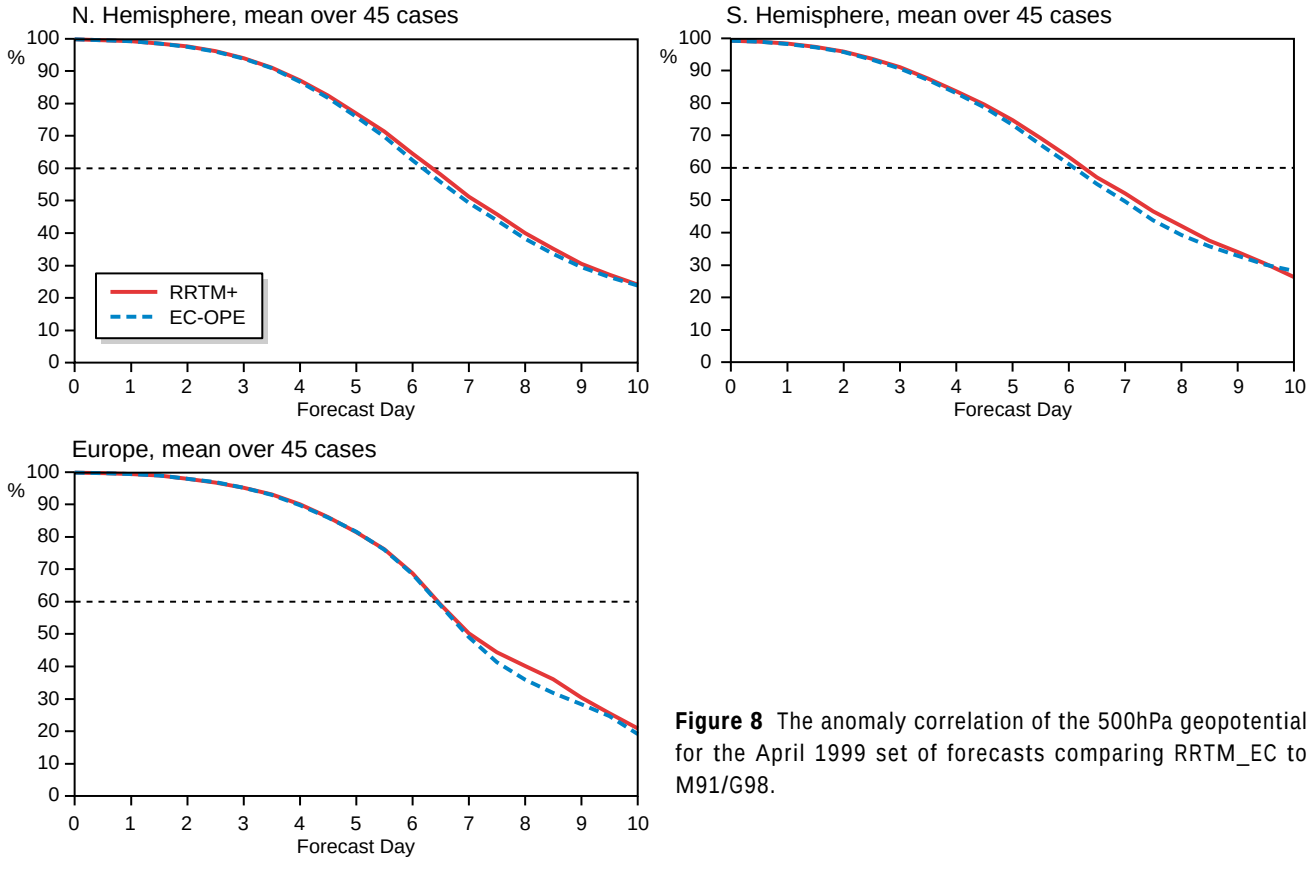

Figure 8 The anomaly correlation of the 500hPa geopotential for the April 1999 set of forecasts comparing RRTM_EC to M91/G98.

RRTM_EC improves the objective scores compared with M91/G98. When considering the corresponding scatter diagrams of Z500 for days 3, 5 and 7 over the northern and southern hemispheres, the centre of gravity of the set of forecasts with RRTM_EC is shifted towards higher correlation, particularly for the Southern Hemisphere results.

Finally, Figure 9 present scores for the Southern Hemisphere for 81 days from the experimental suite just before the operational implementation on 27 June 2000. Over this hemisphere the impact of the new radiation scheme might be seen more clearly than over the Northern Hemisphere where the new surface scheme also has some impact. Improvement is seen in both the anomaly correlation of Z500 and the rms error of the wind at 200 and 850 hPa. A comparison of the time-series of Z500 (Figure 10) shows the improvement to be present for most of the 81 days and over the full length of the forecasts. Although other modifications to the analysis system also play a role, the improvement after day 3 is thought to be linked to the better representation of the radiative processes.

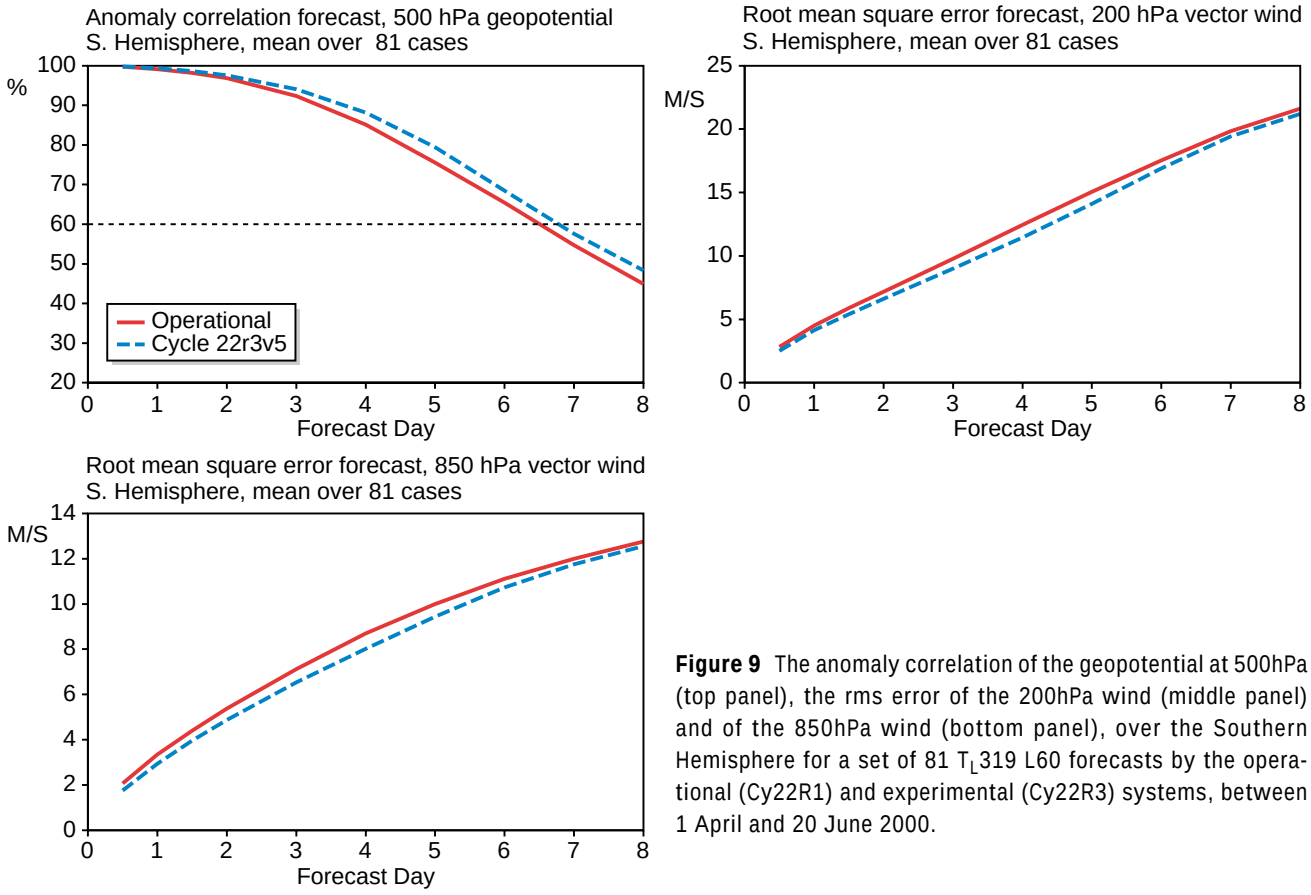

Figure 9 The anomaly correlation of the geopotential at 500hPa (top panel), the rms error of the 200hPa wind (middle panel) and of the 850hPa wind (bottom panel), over the Southern Hemisphere for a set of 81 T_L319 L60 forecasts by the operational (Cy22R1) and experimental (Cy22R3) systems, between 1 April and 20 June 2000.

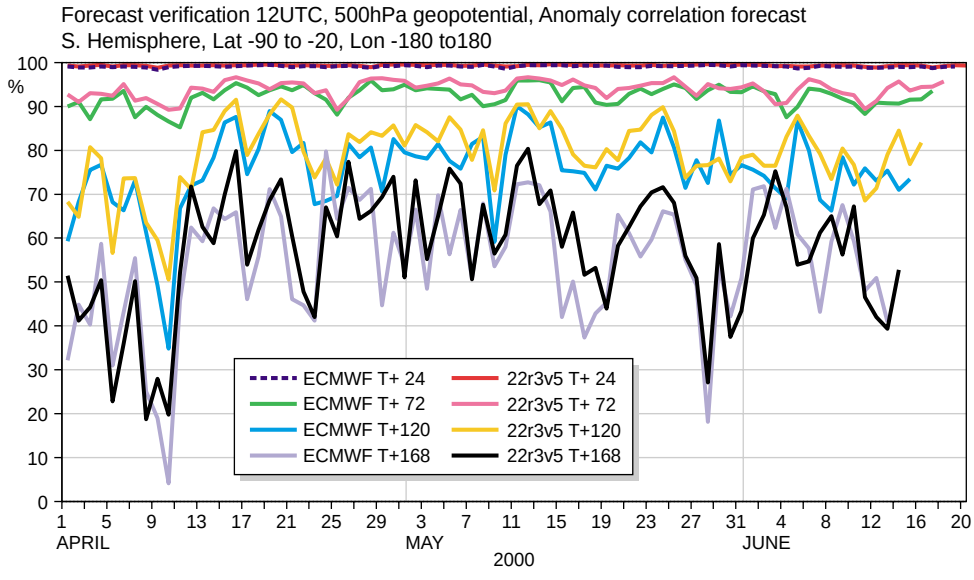

Figure 10 The time series of the anomaly correlation of the geopotential at 500hPa for the Southern Hemisphere, over the 81 days from 1 April to 20 June 2000, with the operational (ECMWF) and experimental (22r3v5) system.

By its derivation from a state-of-the-art line-by-line model validated over several seasons of interferometer observations at both the ARM south Great Plains and north slope of Alaska sites, RRTM certainly offers one of the best possible parametric representations of the clear-sky LW radiative transfer. Its 16 spectral intervals and its less approximate treatment of the cloud layers have also allowed an improved representation of the effects of the cloudiness on the LW fluxes and heating rates. After further optimisation carried out at ECMWF to adapt it to the ECMWF computing environment, RRTM_EC is faster than M91/G98 for 50 and more vertical levels. RRTM_EC has shown essentially positive impact over a large range of parameters, in particular for the surface radiation and the temperature in the stratosphere. Some deficiencies already present in the model with the M91/G98 scheme are somewhat exacerbated by RRTM_EC, particularly in the tropics. However, it is thought that it offers a much better basis for further developments in the ECMWF model.

Acknowledgements

At ECMWF, Deborah Salmond, David Dent, and Mats Hamrud are gratefully acknowledged for providing various 'speeding-up' modifications to the code, and Joao Teixeira for helping with RRTM tests in the one-dimensional version of the ECMWF physics package. □

References

Clough, **S.A.**, **F.X. Kneizys**, and **R.W. Davies**, 1989: Line shape and the water vapour continuum. *Atmos. Res.*, **23**, 229-241.

Clough, **S.A**, **M.J. Iacono**, and **J.-L. Moncet**, 1992: Line-by-line calculation of atmospheric fluxes and cooling rates: Application to water vapour. *J. Geophys. Res.*, *97D*, **15**, 761-15, 786.

Clough, **S.A.**, and **M.J. Iacono**, 1995: Line-by-line calculation of atmospheric fluxes and cooling rates: 2, Application to carbon dioxide, ozone, methane, nitrous oxide and the halocarbons. *J. Geophys. Res.*, *100D*, **16**, 519-16, 536.

Ebert, **E.E.**, and **J.A. Curry**, 1992: A parametrization of ice cloud optical properties for climate models. *J. Geophys. Res.*, *97D*, 3831-3836.

Giorgetta, **M.A.**, and **J.-J. Morcrette**, 1995: Voigt line approximation in the ECMWF radiation scheme. *Mon. Wea. Rev.*, **123**, 3381-3383.

Gregory, **D.**, **J.-J. Morcrette**, **C. Jakob**, and **A. Beljaars**, 1998: Introduction of revised radiation, convection and vertical diffusion schemes into cycle 18r3 of the ECMWF integrated forecasting system. *ECMWF Technical Memorandum No. 254*, 39 pp.

McClatchey, **R.A.**, **R.W. Fenn**, **J.E.A. Selby**, **F.E. Volz**, and **J.S. Garing**, 1971: Optical properties of the atmosphere. AFCRL 71-0279, *Environ. Res. Paper No. 354*, Bedford, Mass., 91 pp. (also 1972, AFCRL-72-0497, ERP 411, 3rd ed., 108pp)

Mlawer, **E.J.**, **S.J. Taubman**, **P.D. Brown**, **M.J. Iacono**, and **S.A. Clough**, 1997: Radiative transfer for inhomogeneous atmospheres: RRTM, a validated correlated-k model for the long-wave. *J. Geophys. Res.*, *102D*, **16**,663-16,682.

Morcrette, **J.-J.**, 1991: Radiation and cloud radiative properties in the ECMWF operational weather forecast model. *J. Geophys. Res.*, *96D*, 9121-9132.

Morcrette, **J.-J.**, **S.A. Clough**, **E.J. Mlawer**, and **M.J. Iacono**, 1998: Impact of a validated radiative transfer scheme, RRTM, on the ECMWF model climate and 10-day forecasts. *ECMWF Technical Memo. No. 252*, 47 pp.

Ohmura, **A.**, **E.G. Dutton**, **B. Forgan**, **C. Frohlich**, **H. Gilgen**, **H. Hegner**, **A. Heimo**, **G. Konig-Langlo**, **B. McArthur**, **G. Muller**, **R. Philipona**, **R. Pinker**, **C.H. Whitlock**, **K. Dehne**, and **M. Wild**, 1998: Baseline Surface Radiation Network (BSRN/WCRP): New precision radiometry for climate research. *Bull. Amer. Meteor. Soc.*, **79**, 2115-2136.

Roberts, **E.E.**, **J.E.A. Selby**, and **L.M. Biberman**, 1976: Infrared continuum absorption by atmospheric water vapour in the 8-12 micron window. *Appl. Opt.*, **15**, 2085-2090.

Smith, **E.A.**, and **Lei Shi**, 1992: Surface forcing of the infrared cooling profile over the Tibetan plateau. Part I: Influence of relative long-wave radiative heating at high altitude. *J. Atmos. Sci.*, **49**, 805-822.

J.-J. Morcrette[1], E.J. Mlawer[2], M.J. Iacono[2], and S.A. Clough[2]
[1] European Centre for Medium-Range Weather Forecasts
[2] Atmospheric and Environmental Research, Inc., Cambridge, USA.

ECMWF wave-model products

Operational global sea-state forecasting started at ECMWF in June 1992. Many changes have been taking place ever since (*Janssen et al.* 1997; *Bidlot et al.* 2000). At present, global and limited-area versions of the wave model (WAM) are run at ECMWF. In its global version, WAM is now a component of the ECMWF atmospheric forecast/analysis system, with surface winds from the atmospheric model provided to WAM on a frequent basis. In addition, the sea-state-dependent drag coefficient is determined from the stress induced by the ocean waves on the airflow (*Janssen 1998*, 1999, 2000a). This two-way coupling between waves and winds was first implemented operationally in June 1998. Since then, it has been included in the different components of the forecasting activities at ECMWF.

Wave model configurations

Products from different configurations of WAM are available at ECMWF (Table 1). Global wave analyses and ten-day deterministic forecasts (from 12 UTC) with an effective resolution of 55 km (*Bidlot and Holt* 1999) are produced daily in conjunction with the T511L60 atmospheric model and the 12-hour 4D-Var analysis system. The wave spectral resolution was upgraded to 30 frequencies (from 0.0345 Hz to 0.548 Hz) and 24 directions at the end of November 2000.

Stream	Domain	Class	Grid	Type	Parameters (see table2)	n_{fre}	n_{ang}
WAVE	Global	od	0.5° ($)	an,4v,fc	220-239,244-248, 251(*)	30	24
WAVE	Mediterranean (+)	od	0.25° ($)	an,fg,fc	220-239,244-248, 251(*)	30	24
WAVE	Global	e4	1.5° (!)	an,fg,fc	220-239,244-248, 251(*)	25	12
WAMO	Global	od	1.5°	an,fc	229, 230, 232, 240-243	30	24
SCWV	Global	od	0.5°	an,fg,fc	220-239,244-248, 251(*)	30	24
WAEF	Global	od	1.0° ($)	cf,pf,fp	220-239, 244, 245, 229, 232	25	12
WAMF	Global (#)	od	1.5° (!)	cf,fc	229-233, 245	25	12
WASF	Global (#)	od	3.0° (!)	fc	229-233, 245	25	12

Table 1 Operationally archived wave products

WAVE – wave daily archive products.
WAMO – monthly mean of wave daily archive products.
SCWV – short cut-off wave archive products.
WAEF – ensemble forecast wave archive products.
WAMF – monthly forecast wave archive products.
WASF – seasonal forecast wave archive products.
an – analysis, 4v – 4D-Var trajectory, fg – first guess, fc – forecast, cf – control forecast,
pf – perturbed forecast, fp – forecast probability.
od – operational data , e4 – era40 products.
n_{fre} – number of frequencies in the spectrum (parameter 251)
n_{ang} – number of directions in the spectrum (parameter 251)
(+) – also known as the limited-area wave model.
($) – irregular latitude/longitude grid.
(*) – 251 is only archived for the analysis and the three-hour forecasts.
(#) – available in the near future.
(!) – uses deep-water physics only.

Analysed wave spectra are archived for all major synoptic times, together with a list of derived integrated parameters (see below) for the analysis and the same forecast steps as the atmospheric fields. Some new parameters have recently been added (Table 2). Note that some products are disseminated to the Member States, but are not archived. For example, forecast wave spectra are provided to the Irish Met Service as boundary conditions for their limited-area WAM (Figure 1).

A higher-resolution limited-area wave model is also run once daily, albeit in uncoupled mode, using global analysed and forecast wind fields from the coupled system. It is an extension of the previous limited-area model, known as the Mediterranean wave model. For this reason, the domain of the model is still referred as Mediterranean even though it covers the whole North Atlantic and all seas around Europe with a 28 km grid spacing. The daily forecasts extend to day 5.

The coupled WAM is also a component of the 40-year reanalysis project. The horizontal resolution is coarser (1.5°) to match the atmospheric model resolution (T159L60). The same parameters as in the daily archive are produced, including the analysed wave spectra (with 25 frequencies and 12 directions).

For statistical purposes, monthly mean of the daily archive is created for a subset of parameters (Tables 1 and 2). It includes statistics on the wave fields as well as on the forcing wind fields.

Recently, the short-cut-off forecast project became operational to provide Member States with boundary conditions for their atmospheric limited-area models. The coupled version of WAM is again included in this system. The same list of parameters as in the daily archive is produced.

The coupled WAM has also been included in the ensemble forecasting system (EPS). Every day, fifty perturbed forecasts and one control forecast are computed with the T255L40 atmospheric model coupled to the wave model. The current WAM resolution is of the order of 110 km with 25 frequencies and 12 directions. The perturbed wave forecasts reflect the uncertainties of the forecasts as introduced into the system by perturbing the initial atmospheric fields only and randomly disturbing the atmospheric physical processes during the forecast integration. Nevertheless, wave probabilistic forecasting is possible and should be further explored. For example, the upper panel in Figure 2 displays the probability (in %) that significant wave heights will exceed 8 m four days in advance. The verifying analysis is shown in the upper right panel. A visual comparison between the two panels indicates that the area of high waves in the Gulf of Biscay was well captured by the EPS. Similarly, the probability that the wave mean periods are larger than 12 seconds is shown in the lower left panel. The corresponding analysis in the lower right panel also indicates the usefulness of EPS wave forecasting. Note that its potential benefit in ship routine has already been demonstrated in a preliminary study (*Hoffschildt et al*. 2000; *Janssen* 2000b).

ECMWF has embarked on the development of operational forecasting systems for the monthly to seasonal range. These systems require the coupling between an ocean-circulation model and a general-circulation model. In its current development configuration, the atmospheric model is also coupled

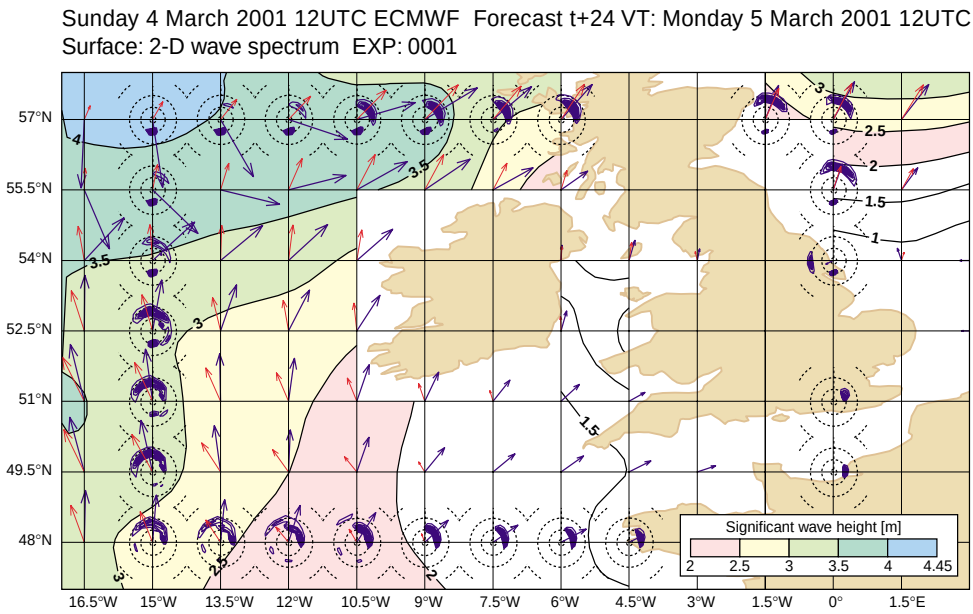

Figure 1 ECMWF global model day 1 forecast for 12 UTC, 5 March 2001 (0.5m contours). The main features of the wave-model spectra are schematically represented on frequency-direction polar plots along the open boundary of the Irish Met Service regional wave model (low-frequency systems are closer to the centre of the plots). At each grid point, the longest arrow denotes the mean propagation direction for the total sea. The shortest arrow represents the mean wind waves. Note that small-wave systems might not have been represented by the contouring program.

Table 2 Archived wave parameters

Code	Abbreviation	Field	Units
220	MP1	Mean wave period from 1st moment	s
221	MP2	Mean wave period from 2nd moment	s
222	WDW	Wave spectral directional spread	–
223	P1WW	Mean wave period from 1st moment of wind waves	s
224	P2WW	Mean wave period from 2nd moment of wind waves	s
225	DWWW	Wave spectral directional spread of wind waves	–
226	P1PS	Mean wave period from 1st moment of swell	s
227	P2PS	Mean wave period from 2nd moment of swell	s
228	DWPS	Wave spectral directional spread of swell	–
229	SWH	Significant wave height	m
230	MWD	Mean wave direction	°
231	PP1D	Peak period of 1d spectra	s
232	MWP	Mean wave period	s
233	CDWW	Coefficient of drag with waves	–
234	SHWW	Significant height of wind waves	m
235	MDWW	Mean direction of wind waves	°
236	MPWW	Mean period of wind waves	s
237	SHPS	Significant height of swell	m
238	MDPS	Mean direction of swell	°
239	MPPS	Mean period of swell	s
240	SDWH	Standard deviation of wave height	m
241	MWS	Monthly mean 10m wind speed	m/s
242	MWD	Monthly mean wind direction	°
243	SDWS	Standard deviation of monthly wind speed	m/s
244	MSQS	Mean square slope	–
245	WIND	10m wind speed modified by wave model	m/s
246	AWH	Altimeter wave height on wave model grid	m
247	ACWH	Corrected altimeter wave height on wave model grid	m
248	ARRC2	Altimeter range relative correction on wave model grid	–
251	2DFD	2-D wave spectra per frequency and direction ***	m^2s/radian

*** The common logarithm of the 2-D wave spectrum is actually encoded.

to WAM; however, there is still no direct coupling between the ocean currents and the waves. Operational monthly forecasts will soon be issued. The corresponding wave products will be computed on a 1.5° grid for a limited number of integrated parameters (Table 1). Similarly, when the new seasonal forecasting system is installed operationally, wave products will be generated on a coarse 3° grid.

Archived wave-model parameters

We now give a short definition of the output wave-model parameters. Note that not all parameters were produced in the past. Please contact our data section for more details. A list of all existing wave model parameters is given in Table 2.

The quantity that is actually computed at each grid point is the two-dimensional wave energy spectrum $F(f,\theta)$, and the total surface stress τ for a given forcing by surface (10 m) winds. In its continuous form, $F(f,\theta)$ describes how the mean sea-surface elevation variance due to waves is distributed in function of frequency (f) and propagation direction (θ). In the numerical implementation of the wave model, F is discretised using n_{fre} frequencies and n_{ang} directions (Table 1). Whenever possible, $F(f,\theta)$ is output and archived as parameter 251, since it corresponds to the full description of the wave field at any grid point, as nicely illustrated in Figure 1. It is, however, a very cumbersome quantity to handle because it is made of ($n_{fre} \times n_{ang}$) scalar fields.

In order to simplify the study of the sea state, integrated parameters have historically been computed from weighted integrals of $F(f,\theta)$ (with the exception of the peak frequency, see later). Also, we differentiate between the wave components that are still under the influence of the local forcing wind, the so-called wind waves (or wind sea), and the rest, referred to as swell. To a good approximation, spectral components are considered to be subject to forcing by the wind when

$$1.2 \times 28 \times (u_* / c) \cos(\theta - \phi) > 1 \,, \qquad (1)$$

where u_* is the friction velocity ($u_*^2 = \tau$), $c = c(f)$ is the phase speed as derived from the linear theory of waves and ϕ is the wind direction. The integrated parameters are computed for wind waves and swell by integrating over the respective components of $F(f,\theta)$ which satisfy (1) or not. Let us define m_n as the integral of $f^n F(f,\theta)$ over f and θ (i.e. the moment of order n of F), and $E(f)$, the frequency spectrum, as the integral of $F(f,\theta)$ over θ only.

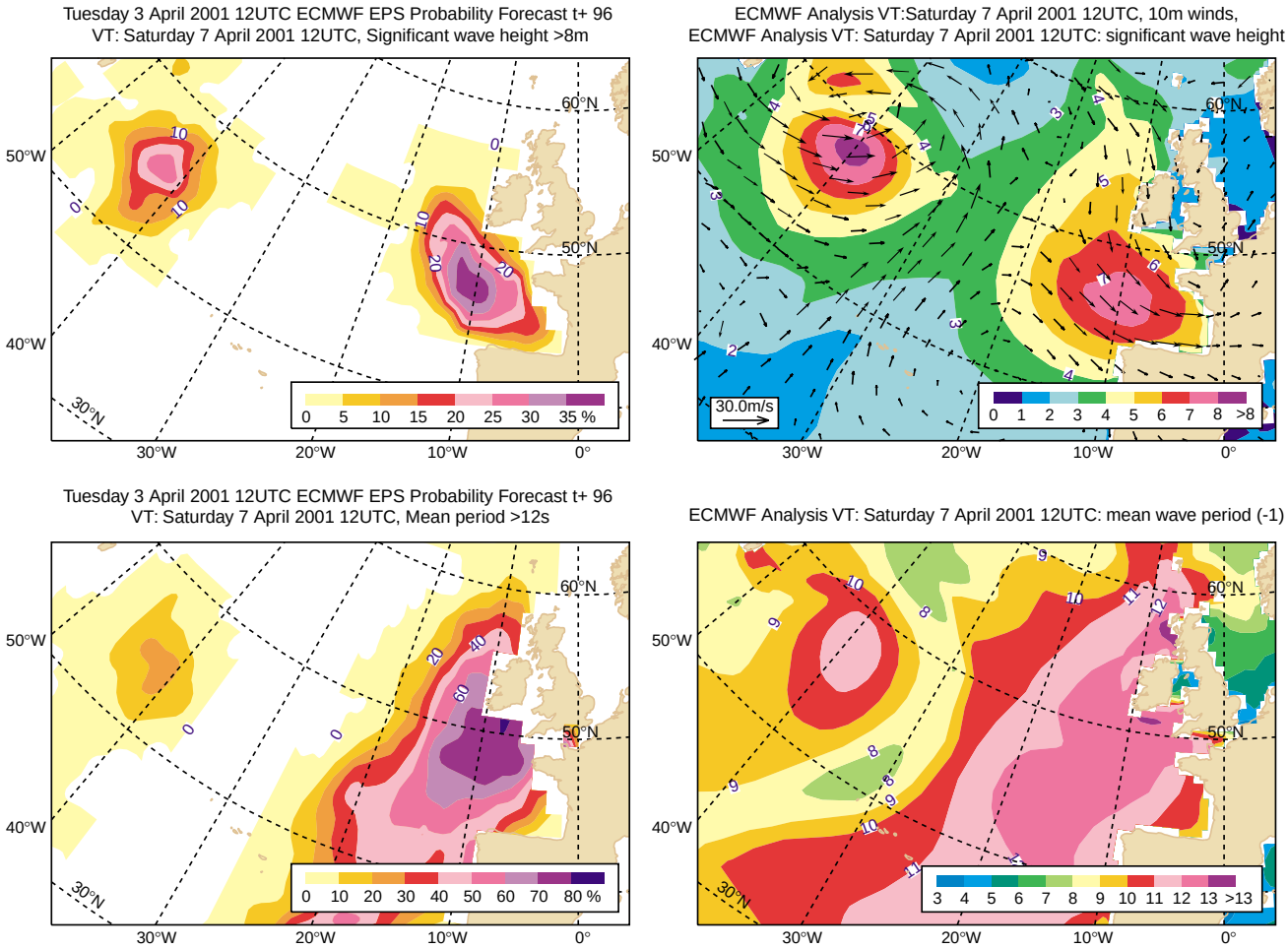

Figure 2 *Left panels*: the probability, in percent, that significant wave heights are larger than 8 m (upper panel) and mean periods are higher than 12 s (lower panel) at 12 UTC 7 April 2001, as derived from the EPS forecast from 12 UTC 3 April.
Right panels: verifying analysis at 12 UTC 7 April 2001 for significant wave heights (colour shading in upper panel) and 10 m winds (arrows) and mean periods (lower panel).

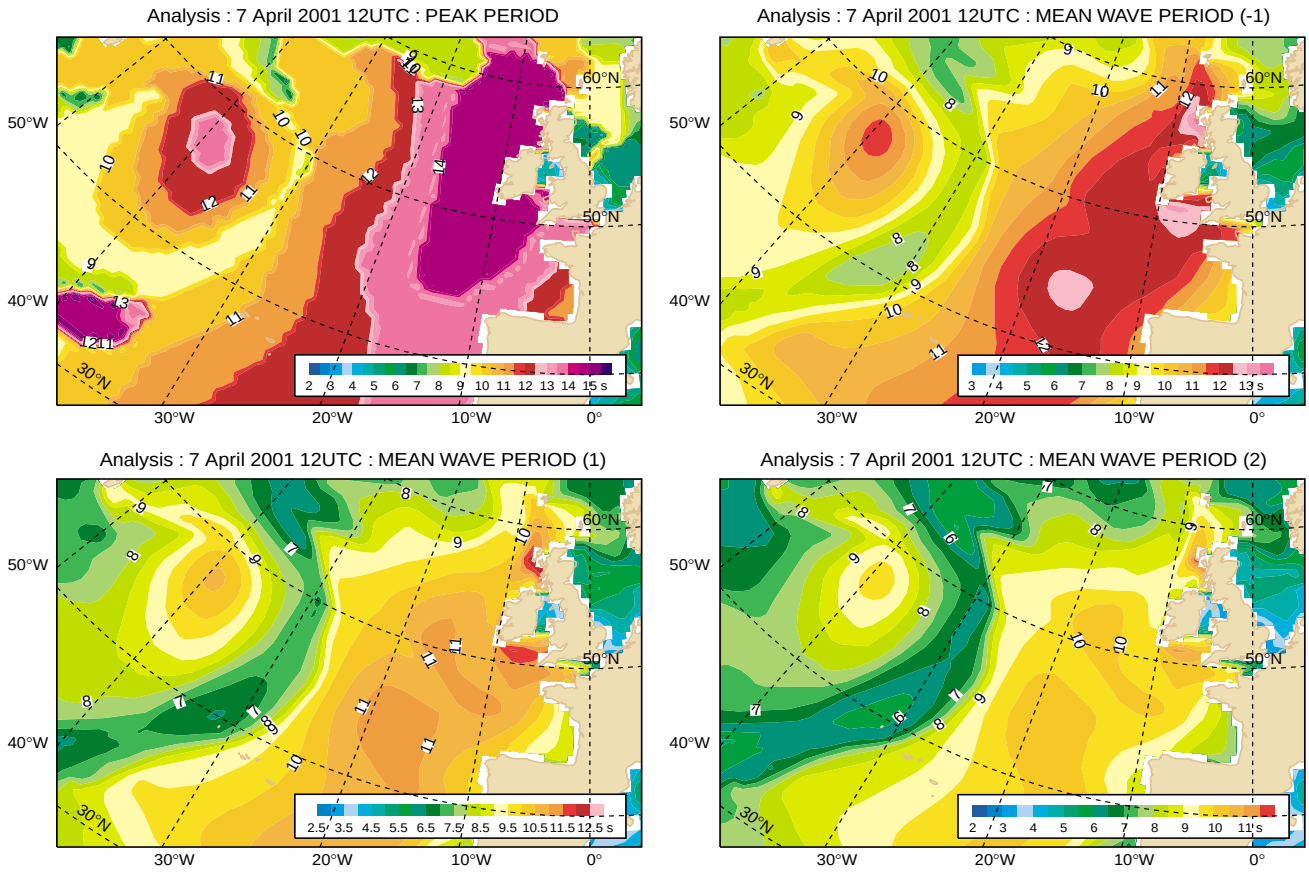

Figure 3 Wave periods analysis for 12 UTC, 7 April 2001, *(see text)*.

The zeroth moment is equal to the mean variance of the sea-surface elevation due to the waves. By definition, the significant wave height (H_s) is given as $H_s = 4 \times (m_0)^{1/2}$.

Since the wave energy spectrum can be derived from observations (by buoys, radar, . . .), the significant wave height can be readily determined by integration of the observed spectrum. It can also be shown that the significant wave height is approximately equal to the average height of the highest-third wave maxima, which is the relevant – or 'significant' – quantity estimated traditionally by means of visual observations of the sea state. Hence the historical origin of the term significant.

The characterisation of a wave system also requires the knowledge of the frequencies or periods of its main components. The peak period is, therefore, defined as the period at which the frequency spectrum $E(f)$ is maximum. The notion of mean period can also be introduced as weighted integrals of the two-dimensional spectrum. Originally, the model mean period (T_{-1}) was based on the moment of order -1, where $T_{-1} = m_{-1}/m_0$.

In order to look at different aspect of the wave field or to compare to observations, other moments can be used to define a mean period. Periods can be based on the first moment $T_1 = m_0/m_1$. Similarly, periods can also be based on the second moment ($T_2 = (m_0/m_2)^{1/2}$), also known as the zero-upcrossing period,

Figure 3 shows the different mean periods for the total sea as defined above for the same situation as in Figure 2.

Since waves propagate, it is useful to characterise them in the first instance with a mean propagation direction. By weighting $F(f,\theta)$, one can defined a mean propagation direction (φ = atan (SF/CF), where SF and CF are, respectively, the integral of $\sin(\theta) \times F(f,\theta)$ and of $\cos(\theta) \times F(f,\theta)$ over f and θ.

For plotting purposes, arrows can be used to represent wave heights (as intensity) and the associated mean propagation direction. For example, the arrows in the upper left panel of Figure 4 illustrate the wind waves and in the lower left panel the remaining swell wave height and propagation direction for the same situation as in Figure 2. The colour shadings represent the corresponding mean period of the wave systems. Note that wind waves tend to be present in regions of rapidly varying winds, whereas the rest of the ocean is mostly swell. Regions of cross-sea where the total wave field is composed of wind waves and swell propagating roughly at 90° can easily be identified (i.e. west of Ireland).

However, a mean propagation direction might not be sufficient to properly describe the propagation characteristics of an ocean wave field. It is customary to view $F(f,\theta)$ as $E(f) \times D(f,\theta)$, where D is the directional distribution. In order to reduce the study of the full directional spectrum to a small number of parameters, the directional distribution of the different wave components can be obtained from the circular standard deviation of D, usually referred to as the directional spread (σ)

$$\sigma = [2(1-r_1)]^{1/2}, \qquad (2)$$

where r_1 is the first-order centred Fourier coefficient of D (note that other directional spreads can be defined based on higher-order Fourier coefficient). In general, r_1 is a function of frequency. If the whole spectrum is considered, a weighted average of the different r_1 can used to conveniently define a mean directional spread. In that case, it can be shown that r_1 can be computed as $r_1 = I_1 / m_0$, where I_1 is the integral of $\cos(\theta - \varphi(f)) \times F(f,\theta)$ over f and θ with $\varphi(f)$ the mean direction at frequency f:

$$\varphi(f) = \text{atan}(\text{sf}(f)/\text{cf}(f)), \qquad (3)$$

where sf(f) and cf(f) are, respectively, the integral of $\sin(\theta) \times F(f,\theta)$ and $\cos(\theta) \times F(f,\theta)$ over θ only.

For wind waves and swell, however, it is preferable to mainly consider the directional spread present at the respective spectral peak. In that case r_1 can be written as $r_1 = I_p / E(f_p)$, where I_p is the integral of $\cos(\theta - \varphi(f_p)) \times F(f_p,\theta)$ over θ only, f_p is the frequency at the respective spectral peak and $\varphi(f_p)$ is given by (3), after $F(f,\theta)$ is split in wind-sea and swell components using (1).

As defined by (2), the mean directional spread σ takes values between 0 and $\sqrt{2}$, where 0 corresponds to a unidirectional spectrum ($r_1 = 1$), and $\sqrt{2}$ to a uniform spectrum ($r_1 = 0$), as illustrated in the upper right panel of Figure 4. This figure complements the wind-sea and swell plots on the directional properties of the wave field.

In the wave model, the surface stress depends on the waves (sea-state dependency). This feature is archived via the drag coefficient (C_d), which relates the surface stress to the square of the wind speed. Note that the sea-state-dependent roughness is also present in the atmospheric model output in the form of the Charnock parameter field (surface parameter 148).

Similarly, an integrated parameter that can be also related to the average slope of the waves is the mean square slope, which is only defined for the total sea as the integral of $k^2 \times F(f,\theta)$ over f and θ, where k is the wave number as given by the linear dispersion relation. The lower right panel in Figure 4 is an example of such a field.

Due to different spatial grids, the forcing winds are interpolated to the wave-model grid. Furthermore, in case of analysed fields, the radar altimeter data-assimilation scheme is such that it produces increments for wave heights, and also for wind speeds. Hence, the wind speed that is actually seen by the wave model can be different from the 10 m wind speed provided by the atmospheric model; it is, therefore, archived. The wind direction is still given by the direction of the input 10 m winds.

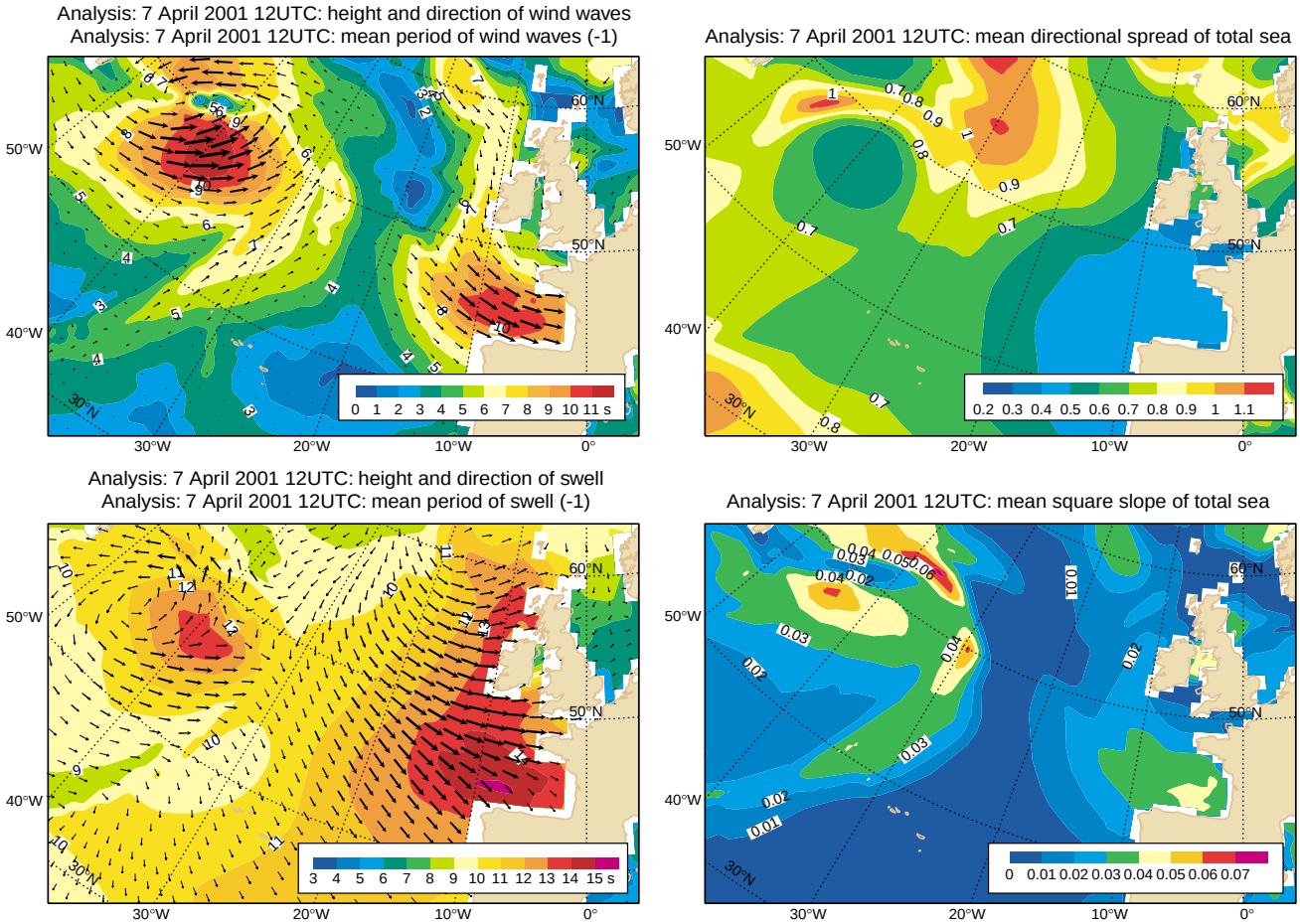

Figure 4 A few selected integrated parameters from the wave model analysis at 12 UTC, 7 April 2001. Upper left panel: wind-wave height and propagation direction (arrows) and mean period (T_{-1}) (colour shadings). Lower left panel: swell-wave height and mean propagation direction (arrows) and mean period (T_{-1}) (colour shadings). Upper right panel: mean directional spread for the total sea. Lower right panel: mean square slope for the total sea.

Even though altimeter data are processed observations, and thus not as such wave model results, their processing has required some information from the model. Following a quality-control procedure that discards all spurious data, the raw altimeter wave height data, which are available in a plus or minus three-hour time window, are collocated at the closest model grid point. The average value is computed for all grid points with at least two individual observations. The averaged data are then archived on the same grid as all wave-model fields.

These gridded altimeter wave heights could, in principle, be used by the wave-model assimilation scheme. However, because of a known underestimation due to the inherent non-Gaussian distribution of the sea-surface elevation, a correction is derived from the model spectra and is added to the altimeter data (*Janssen* 1999, 2000a). The corrected data are used by the assimilation scheme and are archived as such. The altimeter range observation is also affected by the non-Gaussian nature of the sea-surface elevation. A correction can also be derived as a fraction of the observed wave height. This number is also collocated with the wave-model grid and archived. □

References

Bidlot J.-R., **D.J. Holmes**, **P.A. Wittmann**, **R. Lalbeharry**, **H.S. Chen**, 2000: Intercomparison of the performance of operational ocean wave forecasting systems with buoy data. *ECMWF Tech. Memo 315*, ECMWF Reading, UK, 35pp.

Bidlot J.-R. and **M. Holt**, 1999: Numerical wave modelling at operational weather centres. *Coastal Engineering*, **37**, 409-429.

Janssen P.A.E.M., 1998: Progress with wind-wave interaction, *ECMWF Newsletter*, **80**, 2-6.

Janssen P.A.E.M., 1999: Wave modelling and altimeter wave height data. *ECMWF Tech. Memo 269*, ECMWF Reading, UK, 40pp.

Janssen P., 2000a: Wave modelling and altimeter wave height data. in *Satellite Oceanography and Society*, 35-56, edited by D. Halpern, Elsevier Science.

Janssen P.A.E.M., 2000b: Potential benefit of ensemble prediction of waves, *ECMWF Newsletter*, **86**, 3-6.

Janssen P.A.E.M, **B. Hansen** and **J.-R. Bidlot** 1997: Verification of the ECMWF wave forecasting system against buoy and altimeter data. *Wea. Forecasting*, **12**, 763-784.

Hoffschildt M., **J.-R. Bidlot**, **B. Hansen**, **P.A.E.M. Janssen**, 1999: Potential benefit of ensemble forecasts for ship routing. *ECMWF Tech. Memo 287*. ECMWF Reading, UK, 25 pp.

Jean Bidlot

ECMWF publications

Technical Memoranda

321 **E. Klinker** and **L. Ferranti**: Forecasting system performance in summer 1999. Part 1 – Diagnostics related to the forecast performance during spring and summer 1999. *September 2000*

322 **A.J. Simmons**, **E. Andersson**, **M. Fisher**, **C. Jakob**, **G.A. Kelly**, **F. Lalaurette**, **A.P. McNally**, **A. Untch** and **P. Viterbo**: Forecasting system performance in summer 1999. Part 2 Impact of changes to the ECMWF system. *September 2000*

323 **R. Buizza**: Forecasting system performance in summer 1999. Part 3: EPS. *September 2000*

325 **C. Caridinali**: EUCOS impact study. December 2000

327 **J-J. Morcrette**: Assessment of the ECMWF model cloudiness and surface radiation fields at the ARM-SGP site. *January 2001*

328 **I. Gilmour**, **L.A. Smith** and **R. Buizza**: On the duration of the linear regime: Is 24 hours a long time in weather forecasting? *January 2001*

329 **U. Uhrner**: The impact of new sub-grid scale orography fields on the ECMWF model. *January 2001*

330 **P. Bauer**: Rain detection over land surfaces using passive microwave satellite data. *January 2001*

331 **F. Bouttier**: The use of profiler data at ECMWF. *January 2001*

332 **U. Modigliani** and **P. Prior** (Compilers): Report on the twelfth meeting of Member State Computing Representatives, 18-19 May 2000. *February 2001*

333 **R.J. Hogan**, **C Jakob** and **A.J. Illingworth**: Comparison of ECMWF winter-season cloud fraction with radar derived values. *July 2000*

334 **G.J. Marseille** and **F. Bouttier**: Climatologies of sensitive areas for short-term forecast errors over Europe – EUMETNET-EUCOS study. *April 2001*

ECMWF Calendar 2001

Sept 3 – 7	**Seminar** – *Key issues in the parametrization of subgrid-scale processes*	
Oct 1 – 3	**Scientific Advisory Committee**	*30th*
Oct 8 – 10	**Technical Advisory Committee**	*30th*
Oct 15 – 16	**Finance Committee**	*66th*
Oct 18 – 19	**Policy Advisory Committee**	*15th*
Nov 5 – 9	**Workshop** – *Reanalysis*	
Nov 12 – 16	**Eighth ECMWF Workshop on Meteorological Operational Systems**	
Nov 17	**Finance Committee**	*Extraordinary*
Nov 26	**Tech. Advisory Committee**	*Extraordinary*
Dec 10 – 11	**Council**	*55th*